

University of Wollongong

## Research Online

---

Australian Institute for Innovative Materials -  
Papers

Australian Institute for Innovative Materials

---

1-1-2016

### A free-standing graphene-polypyrrole hybrid paper via electropolymerization with an enhanced areal capacitance

Kewei Shu

*University of Wollongong, ks323@uowmail.edu.au*

Caiyun Wang

*University of Wollongong, caiyun@uow.edu.au*

Chen Zhao

*University of Wollongong, cz995@uowmail.edu.au*

Yu Ge

*University of Wollongong, yg711@uowmail.edu.au*

Gordon G. Wallace

*University of Wollongong, gwallace@uow.edu.au*

Follow this and additional works at: <https://ro.uow.edu.au/aiimpapers>



Part of the [Engineering Commons](#), and the [Physical Sciences and Mathematics Commons](#)

---

#### Recommended Citation

Shu, Kewei; Wang, Caiyun; Zhao, Chen; Ge, Yu; and Wallace, Gordon G., "A free-standing graphene-polypyrrole hybrid paper via electropolymerization with an enhanced areal capacitance" (2016). *Australian Institute for Innovative Materials - Papers*. 2195.

<https://ro.uow.edu.au/aiimpapers/2195>

Research Online is the open access institutional repository for the University of Wollongong. For further information contact the UOW Library: [research-pubs@uow.edu.au](mailto:research-pubs@uow.edu.au)

---

## A free-standing graphene-polypyrrole hybrid paper via electropolymerization with an enhanced areal capacitance

### Abstract

Here we developed a free-standing reduced graphene oxide (rGO)-polypyrrole (PPy) hybrid paper via electropolymerization on a paper-like graphene gel. This flexible hybrid paper displayed a uniform layered structure with PPy coated onto the graphene layers. A high areal mass of  $2.7 \text{ mg cm}^{-2}$  could be obtained. It delivered a greatly enhanced areal capacitance of  $440 \text{ mF cm}^{-2}$  at  $0.5 \text{ A g}^{-1}$ , in contrast to that  $151 \sim 198.5 \text{ mF cm}^{-2}$  previously reported for graphene paper or polypyrrole-graphene paper. It can retain  $\sim 81\%$  of the initial capacitance at a high current density of  $6 \text{ A g}^{-1}$ . The combined high flexibility with outstanding electrochemical performance, makes such novel hybrid paper a promising electrode for flexible supercapacitors.

### Disciplines

Engineering | Physical Sciences and Mathematics

### Publication Details

Shu, K., Wang, C., Zhao, C., Ge, Y. & Wallace, G. G. (2016). A free-standing graphene-polypyrrole hybrid paper via electropolymerization with an enhanced areal capacitance. *Electrochimica Acta*, 212 561-571.

# **A Free-standing Graphene-Polypyrrole Hybrid Paper via Electropolymerization with an Enhanced Areal Capacitance**

Kewei Shu, Caiyun Wang\*, Chen Zhao, Yu Ge, Gordon G. Wallace\*

Intelligent Polymer Research Institute, ARC Centre of Excellence for Electromaterials Science, AIIM Facility, Innovation Campus, University of Wollongong, Wollongong, NSW 2522 Australia.

## **\*Corresponding authors**

Tel: +61 2 42981426, Fax: +61 2 4298 1499; E-mail: caiyun@uow.edu.au (C. W.).

Tel: +61 2 42213127, Fax: +61 2 4298 1499; E-mail: gwallace@uow.edu.au (G. W.).

## **Abstract**

Here we developed a free-standing reduced graphene oxide (rGO)-polypyrrole (PPy) hybrid paper via electropolymerization on a paper-like graphene gel. This flexible hybrid paper displayed a uniform layered structure with PPy coated onto the graphene layers. A high areal mass of 2.7 mg cm<sup>-2</sup> could be obtained. It delivered a greatly enhanced areal capacitance of 440 mF cm<sup>-2</sup> at 0.5 A g<sup>-1</sup>, in contrast to that 151~198.5 mF cm<sup>-2</sup> previously reported for graphene paper or polypyrrole-graphene paper. It can retain ~81% of the initial capacitance at a high current density of 6 A g<sup>-1</sup>. The combined high flexibility with outstanding electrochemical performance, makes such novel hybrid paper a promising electrode for flexible supercapacitors.

**Keywords:** Graphene; Areal capacitance; Polypyrrole; Supercapacitor; Flexible hybrid paper electrode

## 1. Introduction

Recently, there is increasing interest in the development of wearable electronic devices, flexible displays and bendable television screens. Such devices require the development of flexible high efficiency energy storage devices [1-3]. Supercapacitors, due to the high power density attainable and excellent cycling stability, are an important class of energy storage devices [4, 5]. An ideal flexible supercapacitor should combine excellent mechanical strength and large electrochemical capacitance. Due to their excellent electrical conductivity, chemical stability and high specific surface area offered by graphene nanosheets, graphene based electrodes in the form of films or papers have shown remarkable flexibility with high gravimetric capacitances in the range of 138 to 210 F g<sup>-1</sup> [6-8].

Although these graphene-based flexible electrodes present promising gravimetric capacitance, they normally deliver a very low areal capacitance in the range of 57 to 94.5 mF cm<sup>-2</sup> due to the low areal mass loading (< 1 mg cm<sup>-2</sup>) [9, 10]. For practical usage, it is suggested that the areal mass loading is at least 5 mg cm<sup>-2</sup> and the electrode thickness is between 50-200 μm [11, 12]. One effective way to improve the areal capacitance is to incorporate metal oxides with high theoretical capacitances. However, graphene/metal oxide hybrid electrodes normally suffer from poor conductivity and excellent performance is only achieved at low scan rates/current densities. A MnO<sub>2</sub>/carbon nanotube/textile nanostructure could deliver a large areal capacitance of 2.8 F cm<sup>-2</sup> at a scan rate of 0.05 mV s<sup>-1</sup>, but this dropped sharply to 120 mF cm<sup>-2</sup> when the scan rate increased to 50 mV s<sup>-1</sup> [13]. A rGO/MnO<sub>2</sub> film electrode showed a capacitance of 245 F g<sup>-1</sup> (i.e. 196 mF cm<sup>-2</sup>) at 2 mV s<sup>-1</sup>. Approximately 58% of the capacitance was observed at 300 mV s<sup>-1</sup> [14]. The use of a 3D graphene/MnO<sub>2</sub> electrode resulted in a large areal capacitance of ~600 mF cm<sup>-2</sup> at 5 mA cm<sup>-2</sup>, but showed a greatly decreased capacitance of 300 mF cm<sup>-2</sup> at 20 mA cm<sup>-2</sup> [15].

Integration of conducting polymers (CPs) with graphene may provide another route to achieve high areal capacitance. In CPs/graphene composites, CPs can provide high pseudocapacitance while graphene can provide a conductive network to overcome the poor cyclic stability of CPs, thus lead to enhanced gravimetric capacitance and good rate performance. Capacitance of  $210 \text{ F g}^{-1}$  (at  $0.3 \text{ A g}^{-1}$ ) and  $285 \text{ F g}^{-1}$  (at  $0.5 \text{ A g}^{-1}$ ) was obtained from polyaniline/graphene film and polypyrrole/sulfonated graphene film, respectively [16, 17]. Polypyrrole (PPy) is one of the most widely used CPs due to its good conductivity, low cost and high charge storage capability [8, 18]. Flexible electrodes based on graphene/PPy composites provide a high gravimetric capacitance ranging from 92 to  $345 \text{ F g}^{-1}$  [19-21] and an areal capacitance in the range of  $152$  to  $175 \text{ mF cm}^{-2}$  [22, 23].

In this work, a novel flexible reduced graphene oxide (rGO)-PPy hybrid paper with an enhanced areal capacitance was developed. PPy was incorporated into a paper-like graphene hydrogel via electropolymerization forming a layered structured rGO-PPy hybrid paper. The rGO-PPy paper with 3 times increased thickness can still keep an equivalent gravimetric capacitance compared to a neat rGO paper. It delivered a much higher areal capacitance of  $440 \text{ mF cm}^{-2}$  at  $0.5 \text{ A g}^{-1}$ , in sharp contrast to  $185 \text{ mF cm}^{-2}$  from a neat rGO paper. The capacitance decreased slightly to  $356 \text{ mF cm}^{-2}$  when the current density was increased to  $6 \text{ A g}^{-1}$ , indicating an excellent rate capability. Compared to the previously reported free-standing graphene-polypyrrole materials, our flexible free-standing rGO-PPy hybrid paper presents a higher areal capacitance and better rate performance.

## **2. Experimental**

### **2.1 Material synthesis**

Graphene oxide (GO) was synthesized from natural graphite flakes by the modified Hummers method. The reduced graphene oxide (rGO) aqueous solution was prepared by

reducing GO solution with hydrazine in the presence of ammonium solution [24]. Typically, ammonium solution (28 wt%, 350  $\mu\text{L}$ ) and hydrazine hydrate (92  $\mu\text{L}$ ) were added to GO dispersion (0.72 mg mL<sup>-1</sup>, 100 mL), and stirred at 95°C for 1 h to complete the reduction. The resultant solution was then subjected to dialysis against a ~0.5 % ammonia solution to remove the excess hydrazine. Paper-like graphene gel was formed via vacuum filtration of rGO solution. This rGO wet gel was peeled off and immersed in water for 6h to remove the impurities.

Prior to PPy electropolymerization, rGO gel was immersed into the aqueous solution of 0.1 M pyrrole and 0.1 M sodium *p*-toluenesulfonate (pTS) overnight at 4 °C. PPy was electrodeposited galvanostatically onto rGO gel at a current density of 1 mA cm<sup>-2</sup> for 20, 40 or 60 min. The obtained rGO-PPy hybrid papers were rinsed with deionized water for several times and then soaked in water overnight to remove the excess monomer or dopant.

## **2.2 Characterization and electrochemical properties**

The surface morphology and cross-sectional view were observed by a field-emission scanning electron microscope (FESEM, JEOL JSM7500FA). The elemental analysis and mapping of the materials were conducted by Bruker X-Flash 4010 energy dispersive X-ray (EDX) detector on FESEM. Raman measurements were performed on a confocal Raman spectrometer (Jobin Yvon HR800, Horiba) utilizing 632.8 nm diode laser. FT-IR spectra were recorded on a FT-IR spectrometer (IRpretige-21, Shimadzu) over the range from 700 to 2000 cm<sup>-1</sup>. The thermal stability was characterized by TGA (Q500, TA instruments), and the measurements were tested under nitrogen at a ramp rate of 5° min<sup>-1</sup>. X-ray photoelectron spectroscopy (XPS) was conducted using XPS system equipped with a hemispherical energy PHOIBOS100/150 analyzer.

The rGO or rGO-PPy paper was assembled into Swagelok-type cell (X2 Labwares Pte Ltd.) to construct symmetric supercapacitor device. The electrolyte used was 1 M H<sub>2</sub>SO<sub>4</sub>. An all solid state supercapacitor was fabricated using PVA-H<sub>3</sub>PO<sub>4</sub> polymer electrolyte following the procedure reported previously [8]. Cyclic voltammetry of the cells was tested using a CHI 650D (CH Instruments, Inc.) and scanned over a range of 0.0 to 1.0 V. Galvanostatic charge/discharge tests were performed using a BTS3000 battery test system (Neware Electronic Co.) over a potential range of 0.005-1.0 V. Electrochemical impedance spectroscopy (EIS) measurements were performed using a Gamry EIS 3000 system, and the frequency range was spanned from 100 kHz to 0.01 Hz with an amplitude of 10 mV at open circuit potential.

### 3. Results and discussion

The procedure used to prepare rGO-PPy paper is summarized in Figure 1a. With the assistance of vacuum filtration, the self-gelation of rGO occurs due to the intersheet  $\pi$ - $\pi$  attractions, forming a lamellar structured graphene wet gel [25]. This gel was then soaked in a pyrrole solution overnight to allow the monomer and dopant to infiltrate into the gel. The polymerization of PPy occurred both on the surface and throughout the gel interior, creating a layered graphene-PPy hybrid structure. The rGO-PPy hybrid papers were named as rGO-PPy20, rGO-PPy40 and rGO-PPy60 according to the deposition time of 20, 40 or 60 min. Their areal mass was 1.80, 2.36 and 2.70 mg cm<sup>-2</sup>, respectively. It was 1.13 mg cm<sup>-2</sup> for the control sample, an unmodified pure rGO paper. The estimated PPy content in rGO-PPy20, rGO-PPy40 and rGO-PPy60 ratio was 37%, 52% and 58%, respectively. Longer deposition time was not necessary since PPy growth tended to saturate after 60 min. The rGO-PPy was flexible, as demonstrated in Figure 1b and can be used directly as binder-free electrode.

The cross-sectional view of rGO paper and rGO-PPy hybrid papers are shown in Figure 2a-c. The rGO paper presents a typical compact layered structure with a thickness of  $\sim 3.7 \mu\text{m}$ , due to the strong  $\pi$ - $\pi$  interaction between graphene sheets (Figure 2a). In contrast, rGO-PPy paper displays an expanded layered structure (Figure 2b, 2c, 2d). PPy acts as spacer between rGO sheets, leading to an enlarged thickness in the range of 12 to 15  $\mu\text{m}$ . All the rGO-PPy papers display similar structure, taking rGO-PPy40 as an example, it clearly shows a lamellar structure with nodule-like PPy on the graphene layers at higher magnification (Figure 2f). An rGO-PPy paper displays a surface morphology with more wrinkles, lumps or islands (Figure 2h) compared to a smoother feature for an rGO paper (Figure 2g).

The elemental analysis of rGO-PPy40 paper surface was detected by EDX module associated with SEM and shown in Figure 3. Only carbon and oxygen elements can be detected on the surface of rGO paper (Figure 3a, b, c). The existence of sulphur and nitrogen elements (originated from PPy/pTS) apart from C and O proves the existence of PPy on the hybrid paper surface (Figure 3d, e, f). The distribution of sulphur element in the cross section of neat rGO or rGO-PPy40 paper was also compared. Very weak sulphur element signal was detected for rGO paper, and it was distributed discretely even at the sample-free area (Figure 3j). Thus the existence of S can be excluded. In contrast, rGO-PPy40 paper displays a clear distribution of sulphur element, evidence of the existence of S (Figure 3l). These results prove that PPy was successfully grown not only on the surface but also the interior of graphene layers. We cannot get a clear mapping image of nitrogen, which may be due to the weak signal of N element.

The successful deposition of PPy can also be confirmed by Raman spectra (Figure 4a). There are only two peaks in the range of  $1000\text{-}2000 \text{ cm}^{-1}$  for neat rGO paper. The peak at around  $1333 \text{ cm}^{-1}$  (D band) is related to the defects and disorder structure in graphene. The peak at  $1593 \text{ cm}^{-1}$  (G band) is ascribed to the doubly degenerate zone centre  $E_{2g}$  mode [26,



27]. Three new peaks can be observed for rGO-PPy paper. The peaks at  $928\text{ cm}^{-1}$  and  $971\text{ cm}^{-1}$  can be assigned to C-H out of plane deformation and PPy ring deformation, respectively. The tiny peak at  $1047\text{ cm}^{-1}$  represents C-H in plane deformation. PPy has characteristic peaks at  $1335\text{ cm}^{-1}$ ,  $1372\text{ cm}^{-1}$  and  $1590\text{ cm}^{-1}$ , which reflect the ring stretching and C=C backbone stretching [28]. Similar to the previously reported graphene/polypyrrole composite materials, they are overlapped with the D-band and G-band of graphene [29]. Since these rGO-PPy samples present similar IR spectra, only the IR spectroscopy from rGO-PPy40 paper are shown (Figure 4c). No obvious peaks were observed for neat rGO paper over the range of  $700\text{-}2000\text{ cm}^{-1}$  in the IR spectroscopy (Figure 4c). The rGO-PPy40 paper exhibits the characteristic adsorption bands of PPy and pTS dopant. The peaks at  $1535$  and  $1446\text{ cm}^{-1}$  are assigned to C=C and C-C stretching of PPy backbone. The band at  $1288\text{ cm}^{-1}$  and  $1026\text{ cm}^{-1}$  corresponds to C-N stretching vibration and C-H, N-H in-plane deformation vibrations, respectively [30, 31]. The band at  $1150\text{ cm}^{-1}$  is due to the stretching vibration of the sulfonate group in pTS [32].

X-ray photoelectron spectroscopy was performed to further investigate the structure of rGO-PPy paper. Figure 4d and 4e show the deconvoluted  $C_{1s}$  spectra of neat rGO and rGO-PPy 40. The  $C_{1s}$  of neat rGO (Figure 4d) can fit into four component peaks, corresponding to different chemical states of carbon. The dominant peak at  $284.7\text{ eV}$  is attributed to the collective effect of  $sp^2$  and  $sp^3$  hybridized carbon [33]. Peaks at  $287.9\text{ eV}$  and  $291.0\text{ eV}$  are assigned to oxygen bonded carbon species, C=O and O-C=O [34]. The peak at around  $286\text{ eV}$  in rGO-PPy  $C_{1s}$  (Figure 4e) corresponds to C-N, C-S and C-O [33]. The intensity of the peak at  $286\text{ eV}$  for rGO-PPy increased remarkably compared to that for neat rGO. It may be ascribed to C-N backbone bonding in polypyrrole. The  $N_{1s}$  core level spectra of rGO-PPy (Figure 4f) was dominated by a main peak at  $399.6\text{ eV}$ , which is assigned to the quinoid imine (=N-) in polypyrrole. The peak at a higher binding energy of  $401.1\text{ eV}$  can be

ascribed to the positively charged protonated nitrogen species [33, 35]. In addition, a  $S_{2p}$  peak arises at 168 eV, which corresponds to sulfonated group in dopant pTS (Figure 4g) [33].

The thermal stability of these papers was investigated using thermal gravimetric analysis (Figure 4h). The weight loss of neat rGO paper over 25-600 °C is about ~10 %, which can be attributed to the decomposition of residual oxygen-containing groups [36]. For pure PPy/pTS film, the major weight loss (45%) occurred at the temperature range of 200~600 °C, which is mainly due to the removal of counter ion pTS [37, 38]. A total weight loss of 19%, 24% and 28% was displayed for rGO-PPy20, rGO-PPy40 and rGO-PPy60, respectively, which is related to the increase amount of PPy.

The capacitive performance of rGO or rGO-PPy paper electrode was studied using cyclic voltammetry (CV) in a three electrode system (Figure 5). No obvious redox peaks were observed for the rGO paper over the potential range -0.5~ 0.5 V (vs. Ag/AgCl) (Figure 5a). The rectangular CV shape indicates a nearly ideal electric double-layer capacitive behaviour. The rGO-PPy electrodes presented features of a pseudocapacitive activity which combining faradic and non-faradic responses. The redox peak of PPy can be observed at around -0.2 V and 0.2 V (Figure 5b, c, d) [39]. This pseudocapacitive behaviour became more significant with the increase amount of PPy.

The paper electrodes were then assembled into symmetric supercapacitors for evaluation. Different from the three electrode system, the rGO-PPy paper based symmetric supercapacitor did not show the remarkable redox peaks of PPy (Figure 6). It is typical for a two-electrode cell system since one electrode was oxidized while its symmetric electrode was reduced, resulting in negligible redox peaks [11, 40]. Over the scan rate range from 20 to 100  $mV s^{-1}$ , all the rGO-PPy papers displayed nearly rectangular CVs even for that with a high areal mass loading of  $2.7 mg cm^{-2}$ . All these reveal their ideal capacitive behaviour. This result is in sharp contrast to that of  $MnO_2$ -graphene paper electrode with similar areal mass

loading but presented highly distorted a CV curve at  $20 \text{ mV s}^{-1}$  [41, 42]. The areal capacitance at  $20 \text{ mV s}^{-1}$  was 298, 349 and  $410 \text{ mF cm}^{-2}$  for rGO-PPy20, rGO-PPy40 and rGO-PPy60, respectively. The rGO-PPy60 paper delivered the highest capacitance, which is over 2 times than that of the neat rGO paper ( $174 \text{ mF cm}^{-2}$  at  $20 \text{ mV s}^{-1}$ ). Our rGO-PPy papers offer much higher areal capacitance than those of the previously reported graphene-PPy film/membrane electrodes, which delivered a lower capacitance ( $151\sim 175 \text{ mF cm}^{-2}$ ) even at a scan rate of  $10 \text{ mV s}^{-1}$  [22, 23, 43].

The charge/discharge tests were performed and the results are shown in Figure 7. Neat rGO delivered a gravimetric capacitance of  $164 \text{ F g}^{-1}$  at  $0.5 \text{ A g}^{-1}$ . It slightly decreased to  $156 \text{ F g}^{-1}$  at  $2 \text{ A g}^{-1}$ . The rGO-PPy20 paper showed the highest gravimetric capacitance among these hybrid papers,  $190 \text{ F g}^{-1}$  at  $0.5 \text{ A g}^{-1}$  and  $165 \text{ F g}^{-1}$  at  $2 \text{ A g}^{-1}$ . The rGO-PPy 40 and rGO-PPy 60 paper delivered a slightly decreased gravimetric capacitance of  $163 \text{ F g}^{-1}$  and  $161 \text{ F g}^{-1}$  at  $0.5 \text{ A g}^{-1}$ , but still comparable to the rGO papers in this work or the previously reported [6, 7, 18]. Benefited from the unique layered structure, rGO-PPy paper with 3 times thickness and much higher mass loading still keeps the similar gravimetric capacitance compared to neat rGO paper.

The areal capacitance of neat rGO and rGO-PPy hybrid papers can be calculated from their gravimetric capacitance and areal mass. The areal capacitance of rGO-PPy hybrid paper increases with the prolonged electrodeposition time. The rGO-PPy 60 paper gave the highest areal capacitance of  $440 \text{ mF cm}^{-2}$  at  $0.5 \text{ A g}^{-1}$ , which was 2.4 times higher than that  $185 \text{ mF cm}^{-2}$  of rGO paper. Meanwhile, rGO-PPy40 and rGO-PPy20 papers showed an areal capacitance of 380 and  $342 \text{ mF cm}^{-2}$ , respectively. It should be pointed out that the current  $0.5 \text{ A g}^{-1}$  was equal to that of 1.35, 1.18, 0.9,  $0.57 \text{ mA cm}^{-2}$  in an areal unit for rGO-PPy60, rGO-PPy40, rGO-PPy20 and rGO paper, respectively. The areal capacitance delivered from our rGO-PPy paper is higher than that from the flexible graphene/PPy fibre electrode (107

mF cm<sup>-2</sup> at 0.24 mA cm<sup>-2</sup>) [44] and carbon fibre/PPy paper electrode (198.5 mF cm<sup>-2</sup> at 1 mA cm<sup>-2</sup>) [45]. At a high current density of 6 A g<sup>-1</sup> (~16 mA cm<sup>-2</sup>), over 300 mF cm<sup>-2</sup> was retained for rGO-PPy60 paper, 81 % of that obtained at 0.5 A g<sup>-1</sup> (Figure 7e). Our rGO-PPy papers present better rate capability compared to the carbon fibre/PPy paper electrode, which demonstrated a capacity retention of only 66% when the current density increased from 1 to 10 mA cm<sup>-2</sup> [45]. This unique PPy coated graphene layered structure ensured excellent rate performance of the rGO-PPy hybrid paper.

The cycle stability of rGO-PPy hybrid papers or neat rGO paper was tested at a current density of 2 A g<sup>-1</sup> (Figure 7f). A capacitance retention of 75%, 78%, 85% and 92% was shown during the first 1000 cycles for rGO-PPy60, rGO-PPy40, rGO-PPy20 and rGO, respectively. A lower retention rate with the increased PPy ratio may be attributed to the decreased pseudocapacitance contribution from PPy. PPy suffers from physical changes associated with the doping/de-doping of ions during cycling [46, 47]. The repeated redox cycles can damage PPy molecule structure and promote PPy degradation, leading to the capacitance decay. It should be pointed out that these rGO-PPy hybrid papers can still retain 71-80 % of the initial capacitance after 5000 cycles, comparable to or higher than that 56~87% retention of the previously reported results for PPy or carbon-PPy based electrodes [48-51].

The areal energy density and power density in the Ragone plot (Figure 8) are calculated using the following equations:  $E = C_s \Delta V^2 / 7200$ ,  $P = 3600E/t$ . The rGO-PPy60 paper presented a maximum energy density of 61.3  $\mu\text{Wh cm}^{-2}$  at a power density of 1.2 mW cm<sup>-2</sup>, while it maintained 49.5  $\mu\text{Wh cm}^{-2}$  at 14.2 mW cm<sup>-2</sup>. Our rGO-PPy paper displayed higher energy density compared to the reported results for graphene paper [10], graphene-polypyrrole film [23], graphene-PANI paper [52], or even graphene-MnO<sub>2</sub> electrode [41] especially at high power density.

The Nyquist plots of a neat rGO or rGO-PPy paper-based electrode were obtained in the frequency range between 0.01 and 100 kHz, and are shown in Figure 9a. An equivalent circuit model is used to fit the impedance spectra (Figure 8a inset). The equivalent series resistance (ESR) includes solution resistance  $R_s$ , electrode-electrolyte interfacial double layer resistance  $R_{dl}$  and charge transfer resistance  $R_{ct}$  [46, 53]. The semi-circle portion in the high frequency region represents two constant phase elements  $CPE_{dl}$  and  $CPE_f$ , accounting for imperfect double layer capacitance and faradic pseudocapacitance. The ESR of our rGO-PPy papers was around 3.5~5.5  $\Omega$ , close to that 2.2  $\Omega$  for the rGO paper. At low frequency region, more vertical plot at low frequency region indicates more ideal capacitive performance [54]. All the rGO and rGO-PPy papers showed nearly vertical line in this region, indicating their good capacitive performances. The rGO paper gave the most vertical plot among those papers, which can be ascribed to the fastest ion and electron transportation due to the lowest layer thickness.

Dynamic electrosorption analysis (DEA) is an effective electrochemical method used to study ion adsorption and transport behaviour in bulk graphene based materials [55]. The relative ion-transport rate within a porous electrode can be implied from a characteristic relaxation time constant  $\tau_0$ , the reciprocal of the frequency where the capacitance is 50% of its maximum value [56, 57]. The increase of  $\tau_0$  is largely attributed to the reduced average pore size. The  $\tau_0$  of rGO-PPy papers was around 1.8 to 2.5 s, slightly higher than that of a neat rGO paper (1.25 s) (Figure 9b). Nevertheless, the  $\tau_0$  offered by rGO-PPy paper based device is comparable to that 0.92-2.27 s for graphene paper based supercapacitors [55], indicating a good porosity for electrolyte to access.

The performance of an all solid-state supercapacitor based on rGO-PPy40 electrodes using polymer electrolyte PVA-H<sub>3</sub>PO<sub>4</sub> was also investigated. Nearly triangular charge/discharge curves at the unbent state with a slightly lower gravimetric capacitance

compared with that with liquid electrolyte (Figure 10a), 140, 118, 96 F g<sup>-1</sup> at 0.5, 1 and 2 A g<sup>-1</sup>, respectively were obtained. That may be ascribed to the decreased ion diffusion or transport within the polymer electrolyte. The capacitive behavior at the bent state was nearly the same as that at the relaxed state (Figure 10b). It can retain 99% and 97% of its capacitance when it was bent 90° and 180°, indicating the robustness of this flexible supercapacitor.

#### **4. Conclusion**

Wet graphene gel was used to prepare free standing graphene/PPy hybrid papers via electropolymerization. PPy was uniformly coated onto the surface and interior of the graphene gel, creating a layered graphene/PPy structure with an increased thickness. The areal mass loading of the hybrid paper can be easily controlled by adjusting the electrodeposition time. Benefiting from this unique structure, these hybrid papers with enlarged thickness showed a gravimetric capacitance comparable to the graphene paper yet with a much higher areal capacitance. This hybrid paper also exhibited excellent rate performance. The high areal-normalized power density and high energy density make such flexible hybrid papers promising materials for the application in flexible energy storage devices.

#### **Acknowledgements**

Funding from the Australian Research Council Centre of Excellence Scheme (Project Number CE 140100012) is gratefully acknowledged. The authors also acknowledge the Australian National Fabrication Facility-Materials node (ANFF) and UOW Electron Microscopy Centre for their provision of research facilities. Gordon G. Wallace is grateful to the ARC for support under the Australian Laureate Fellowship scheme (FL110100196).

Kewei Shu and Chen Zhao acknowledge the support of the CSC scholarship from the Ministry of Education of P. R. China. The authors also thank Dr. Chong-Yong Lee for his critical proof-reading.

## References

- [1] H. Nishide, K. Oyaizu, *Materials science - Toward flexible batteries*, *Science*, 319 (2008) 737-738.
- [2] X. Lu, M. Yu, G. Wang, Y. Tong, Y. Li, *Flexible solid-state supercapacitors: design, fabrication and applications*, *Energy & Environmental Science*, 7 (2014) 2160-2181.
- [3] D. Yang, A. Velamakanni, G. Bozoklu, S. Park, M. Stoller, R.D. Piner, S. Stankovich, I. Jung, D.A. Field, C.A. Ventrice Jr, R.S. Ruoff, *Chemical analysis of graphene oxide films after heat and chemical treatments by X-ray photoelectron and Micro-Raman spectroscopy*, *Carbon*, 47 (2009) 145-152.
- [4] M. Winter, R.J. Brodd, *What Are Batteries, Fuel Cells, and Supercapacitors?*, *Chemical Reviews*, 104 (2004) 4245-4270.
- [5] R. Kotz, M. Carlen, *Principles and Applications of Electrochemical Capacitors*, *Electrochimica Acta*, 45 (2000) 2483-2498.
- [6] M.F. El-Kady, V. Strong, S. Dubin, R.B. Kaner, *Laser Scribing of High-Performance and Flexible Graphene-Based Electrochemical Capacitors*, *Science*, 335 (2012) 1326-1330.
- [7] X. Yang, C. Cheng, Y. Wang, L. Qiu, D. Li, *Liquid-Mediated Dense Integration of Graphene Materials for Compact Capacitive Energy Storage*, *Science*, 341 (2013) 534-537.
- [8] K. Shu, C. Wang, S. Li, C. Zhao, Y. Yang, H. Liu, G. Wallace, *Flexible Free-standing Graphene Paper with Interconnected Porous Structure for Energy Storage*, *Journal of Materials Chemistry A*, 3 (2015) 4428-4434.

- [9] X. Yang, J. Zhu, L. Qiu, D. Li, Bioinspired Effective Prevention of Restacking in Multilayered Graphene Films: Towards the Next Generation of High-Performance Supercapacitors, *Advanced Materials*, 23 (2011) 2833-2838.
- [10] G. Wang, X. Sun, F. Lu, H. Sun, M. Yu, W. Jiang, C. Liu, J. Lian, Flexible Pillared Graphene-Paper Electrodes for High-Performance Electrochemical Supercapacitors, *Small*, 8 (2012) 452-459.
- [11] M.D. Stoller, R.S. Ruoff, Best practice methods for determining an electrode material's performance for ultracapacitors, *Energy & Environmental Science*, 3 (2010) 1294-1301.
- [12] S. Zhang, N. Pan, Supercapacitors Performance Evaluation, *Advanced Energy Materials*, (2014) 1401401(1401401-1401419).
- [13] L. Hu, W. Chen, X. Xie, N. Liu, Y. Yang, H. Wu, Y. Yao, M. Pasta, H.N. Alshareef, Y. Cui, Symmetrical MnO<sub>2</sub>-Carbon Nanotube-Textile Nanostructures for Wearable Pseudocapacitors with High Mass Loading, *ACS Nano*, 5 (2011) 8904-8913.
- [14] Y. Zhao, Y. Meng, H. Wu, Y. Wang, Z. Wei, X. Li, P. Jiang, In situ anchoring uniform MnO<sub>2</sub> nanosheets on three-dimensional macroporous graphene thin-films for supercapacitor electrodes, *RSC Advances*, 5 (2015) 90307-90312.
- [15] Z. Zhang, K. Chi, F. Xiao, S. Wang, Advanced solid-state asymmetric supercapacitors based on 3D graphene/MnO<sub>2</sub> and graphene/polypyrrole hybrid architectures, *Journal of Materials Chemistry A*, 3 (2015) 12828-12835.
- [16] A. Liu, C. Li, H. Bai, G. Shi, Electrochemical Deposition of Polypyrrole/Sulfonated Graphene Composite Films, *The Journal of Physical Chemistry C*, 114 (2010) 22783-22789.
- [17] Q. Wu, Y. Xu, Z. Yao, A. Liu, G. Shi, Supercapacitors Based on Flexible Graphene/Polyaniline Nanofiber Composite Films, *ACS Nano*, 4 (2010) 1963-1970.
- [18] F. Liu, S. Song, D. Xue, H. Zhang, Folded Structured Graphene Paper for High Performance Electrode Materials, *Advanced Materials*, 24 (2012) 1089-1094.



- [19] A. Davies, P. Audette, B. Farrow, F. Hassan, Z. Chen, J.-Y. Choi, A. Yu, Graphene-Based Flexible Supercapacitors: Pulse-Electropolymerization of Polypyrrole on Free-Standing Graphene Films, *Journal of Physical Chemistry C*, 115 (2011) 17612-17620.
- [20] H.P. de Oliveira, S.A. Sydlik, T.M. Swager, Supercapacitors from Free-Standing Polypyrrole/Graphene Nanocomposites, *The Journal of Physical Chemistry C*, 117 (2013) 10270-10276.
- [21] L. Wu, W. Li, P. Li, S. Liao, S. Qiu, M. Chen, Y. Guo, Q. Li, C. Zhu, L. Liu, Powder, Paper and Foam of Few-Layer Graphene Prepared in High Yield by Electrochemical Intercalation Exfoliation of Expanded Graphite, *Small*, 10 (2014) 1421-1429.
- [22] J. Zhang, P. Chen, B.H.L. Oh, M.B. Chan-Park, High Capacitive Performance of Flexible and Binder-free Graphene-polypyrrole Composite Membrane based on In situ Reduction of Graphene Oxide and Self-assembly, *Nanoscale*, 5 (2013) 9860-9866.
- [23] H. Zhou, G. Han, Y. Xiao, Y. Chang, H.-J. Zhai, Facile Preparation of Polypyrrole/graphene Oxide Nanocomposites with Large Areal Capacitance using Electrochemical Codeposition for Supercapacitors, *Journal of Power Sources*, 263 (2014) 259-267.
- [24] D. Li, M.B. Muller, S. Gilje, R.B. Kaner, G.G. Wallace, Processable aqueous dispersions of graphene nanosheets, *Nat Nano*, 3 (2008) 101-105.
- [25] X. Yang, L. Qiu, C. Cheng, Y. Wu, Z.-F. Ma, D. Li, Ordered Gelation of Chemically Converted Graphene for Next-Generation Electroconductive Hydrogel Films, *Angewandte Chemie International Edition*, 50 (2011) 7325-7328.
- [26] A.C. Ferrari, J.C. Meyer, V. Scardaci, C. Casiraghi, M. Lazzeri, F. Mauri, S. Piscanec, D. Jiang, K.S. Novoselov, S. Roth, A.K. Geim, Raman Spectrum of Graphene and Graphene Layers, *Physical Review Letters*, 97 (2006).

- [27] F. Tuinstra, J.L. Koenig, Raman Spectrum of Graphite, *The Journal of Chemical Physics*, 53 (1970) 1126-1130.
- [28] Y.-C. Liu, B.-J. Hwang, W.-J. Jian, R. Santhanam, In situ Cyclic Voltammetry-surface-enhanced Raman Spectroscopy: Studies on the Doping–undoping of Polypyrrole Film, *Thin Solid Films*, 374 (2000) 85-91.
- [29] Y. Yang, C.Y. Wang, B.B. Yue, S. Gambhir, C.O. Too, G.G. Wallace, Electrochemically Synthesized Polypyrrole/Graphene Composite Film for Lithium Batteries, *Advanced Energy Materials*, 2 (2012) 266-272.
- [30] R. Kostić, D. Raković, S.A. Stepanyan, I.E. Davidova, L.A. Gribov, Vibrational spectroscopy of polypyrrole, theoretical study, *The Journal of Chemical Physics*, 102 (1995) 3104-3109.
- [31] J. Stejskal, M. Trchova, I.A. Ananieva, J. Janca, J. Prokes, S. Fedorova, I. Sapurina, Poly(aniline-co-pyrrole): powders, films, and colloids. Thermophoretic mobility of colloidal particles, *Synthetic Metals*, 146 (2004) 29-36.
- [32] C. Guanggui, D. Jianning, Z. Zhongqiang, L. Zhiyong, P. Huasheng, Study on the preparation and multiproperties of the polypyrrole films doped with different ions, *Surface and Interface Analysis*, 44 (2012) 844-850.
- [33] Y.S. Lim, Y.P. Tan, H.N. Lim, W.T. Tan, M.A. Mahnaz, Z.A. Talib, N.M. Huang, A. Kassim, M.A. Yarmo, Polypyrrole/graphene composite films synthesized via potentiostatic deposition, *Journal of Applied Polymer Science*, 128 (2013) 224-229.
- [34] F. Fusalba, D. Bélanger, Electropolymerization of Polypyrrole and Polyaniline–Polypyrrole from Organic Acidic Medium, *The Journal of Physical Chemistry B*, 103 (1999) 9044-9054.

- [35] H.-T. Lee, Y.-C. Liu, Catalytic electrooxidation pathway for the polymerization of polypyrrole in the presence of ultrafine silver nanoparticles, *Polymer*, 46 (2005) 10727-10732.
- [36] S. Park, K.-S. Lee, G. Bozoklu, W. Cai, S.T. Nguyen, R.S. Ruoff, Graphene Oxide Papers Modified by Divalent Ions—Enhancing Mechanical Properties via Chemical Cross-Linking, *ACS Nano*, 2 (2008) 572-578.
- [37] R. Ansari, G.G. Wallace, Effect of thermal treatment on the electrochemical properties of conducting polypyrrole polymers, *Polymer*, 35 (1994) 2372-2377.
- [38] Y. Yang, C. Wang, S. Ashraf, G.G. Wallace, Polypyrrole doped with redox-active poly(2-methoxyaniline-5-sulfonic acid) for lithium secondary batteries, *RSC Advances*, 3 (2013) 5447-5452.
- [39] Y. Tian, F. Yang, W. Yang, Redox behavior and stability of polypyrrole film in sulfuric acid, *Synthetic Metals*, 156 (2006) 1052-1056.
- [40] P. Liu, Y. Huang, Synthesis of reduced graphene oxide-conducting polymers-Co<sub>3</sub>O<sub>4</sub> composites and their excellent microwave absorption properties, *RSC Advances*, 3 (2013) 19033-19039.
- [41] A. Sumboja, C.Y. Foo, X. Wang, P.S. Lee, Large Areal Mass, Flexible and Free-Standing Reduced Graphene Oxide/Manganese Dioxide Paper for Asymmetric Supercapacitor Device, *Adv. Mater.*, 25 (2013) 2809-2815.
- [42] T. Zhai, F. Wang, M. Yu, S. Xie, C. Liang, C. Li, F. Xiao, R. Tang, Q. Wu, X. Lu, Y. Tong, 3D MnO<sub>2</sub>-Graphene Composites with Large Areal Capacitance for High-performance Asymmetric Supercapacitors, *Nanoscale*, 5 (2013) 6790-6796.
- [43] P.A. Mini, A. Balakrishnan, S.V. Nair, K.R.V. Subramanian, Highly Super Capacitive Electrodes Made of Graphene/poly(pyrrole), *Chemical Communications*, 47 (2011) 5753-5755.

- [44] X. Ding, Y. Zhao, C. Hu, Y. Hu, Z. Dong, N. Chen, Z. Zhang, L. Qu, Spinning Fabrication of Graphene/polypyrrole Composite Fibers for All-solid-state, Flexible Fibriform Supercapacitors, *Journal of Materials Chemistry A*, 2 (2014) 12355-12360.
- [45] C.Y. Yang, J.L. Shen, C.Y. Wang, H.J. Fei, H. Bao, G.C. Wang, All-solid-state Asymmetric Supercapacitor Based on Reduced Graphene oxide/carbon nanotube and Carbon fiber paper/polypyrrole Electrodes, *Journal of Materials Chemistry A*, 2 (2014) 1458-1464.
- [46] G.A. Snook, P. Kao, A.S. Best, Conducting-polymer-based supercapacitor devices and electrodes, *Journal of Power Sources*, 196 (2011) 1-12.
- [47] J. Zhang, X.S. Zhao, Conducting Polymers Directly Coated on Reduced Graphene Oxide Sheets as High-Performance Supercapacitor Electrodes, *The Journal of Physical Chemistry C*, 116 (2012) 5420-5426.
- [48] M. Beidaghi, C. Wang, Micro-supercapacitors Based on Three Dimensional Interdigital Polypyrrole/C-MEMS Electrodes, *Electrochimica Acta*, 56 (2011) 9508-9514.
- [49] C. Zhao, C. Wang, R. Gorkin Iii, S. Beirne, K. Shu, G.G. Wallace, Three Dimensional (3D) Printed Electrodes for Interdigitated Supercapacitors, *Electrochemistry Communications*, 41 (2014) 20-23.
- [50] F. Zhang, F. Xiao, Z.H. Dong, W. Shi, Synthesis of Polypyrrole Wrapped Graphene Hydrogels Composites as Supercapacitor Electrodes, *Electrochimica Acta*, 114 (2013) 125-132.
- [51] X. Lu, H. Dou, C. Yuan, S. Yang, L. Hao, F. Zhang, L. Shen, L. Zhang, X. Zhang, Polypyrrole/carbon nanotube Nanocomposite Enhanced the Electrochemical Capacitance of Flexible Graphene Film for Supercapacitors, *Journal of Power Sources*, 197 (2012) 319-324.
- [52] H. Wei, J. Zhu, S. Wu, S. Wei, Z. Guo, Electrochromic Polyaniline/graphite Oxide Nanocomposites with Endured Electrochemical Energy Storage, *Polymer*, 54 (2013) 1820-1831.

- [53] H. Fu, Z.-j. Du, W. Zou, H.-q. Li, C. Zhang, Carbon nanotube reinforced polypyrrole nanowire network as a high-performance supercapacitor electrode, *Journal of Materials Chemistry A*, 1 (2013) 14943-14950.
- [54] R. Kötz, M. Hahn, R. Gallay, Temperature Behavior and Impedance Fundamentals of Supercapacitors, *Journal of Power Sources*, 154 (2006) 550-555.
- [55] J. Zhu, C. Cheng, X. Yang, Y. Wang, L. Qiu, D. Li, Dynamic Electrosorption Analysis as an Effective Means to Characterise the Structure of Bulk Graphene Assemblies, *Chemistry – A European Journal*, 19 (2013) 3082-3089.
- [56] A. Kajdos, A. Kvit, F. Jones, J. Jagiello, G. Yushin, Tailoring the Pore Alignment for Rapid Ion Transport in Microporous Carbons, *Journal of the American Chemical Society*, 132 (2010) 3252-3253.
- [57] P.L. Taberna, P. Simon, J.F. Fauvarque, Electrochemical Characteristics and Impedance Spectroscopy Studies of Carbon-carbon Supercapacitors, *Journal of the Electrochemical Society*, 150 (2003) A292-A300.

## Captions for Figures

Figure 1 (a) Schematic procedures to fabricate a rGO-PPy paper include the following steps: formation of a wet rGO paper via filtration, soaking the wet paper in pyrrole monomer solution, PPy electropolymerization followed by drying. (b) Digital image of a rGO-PPy40 paper

Figure 2 SEM images of the cross section of a neat rGO (a), rGO-PPy20 (b), rGO-PPy40 (c) and rGO-PPy60 paper (d); Surface morphology and cross-sectional view of a neat rGO (e, g) and rGO-PPy40 paper (f, h) at higher magnification.

Figure 3 Element analysis of a neat rGO (a, b surface; g, h cross section) and rGO-PPy40 paper (d, e surface; j, k cross section). Element mapping of the surface of neat rGO (c), rGO-PPy40 (f), and the cross section of rGO (i) and rGO-PPy40 (l).

Figure 4 Raman spectra of a neat rGO or rGO-PPy40 paper (a) and the expanded view over 500~1200  $\text{cm}^{-1}$  (b); IR spectra of a neat rGO or rGO-PPy40 paper (c); XPS spectra of  $\text{C}_{1s}$  in neat rGO (d),  $\text{C}_{1s}$  in rGO-PPy (e),  $\text{N}_{1s}$  in rGO-PPy40 (f) and  $\text{S}_{2p}$  in rGO-PPy (g) (black line, experimental data; colour line: fitting line); TGA curves of neat rGO and rGO-PPy papers (h)

Figure 5 Cyclic voltammograms of a rGO (a), rGO-PPy20 (b), rGO-PPy40 (c) or rGO-PPy60 (d) paper in 1 M  $\text{H}_2\text{SO}_4$  between -0.5 to 0.5 V (vs. Ag/AgCl) at scan rates of 20, 50, 100  $\text{mV s}^{-1}$ .

Figure 6 Cyclic voltammograms of a rGO (a), rGO-PPy20 (b), rGO-PPy40 (c) or rGO-PPy60 (d) paper based supercapacitors in 1 M  $\text{H}_2\text{SO}_4$  at scan rates of 20, 50, 100  $\text{mV s}^{-1}$ .

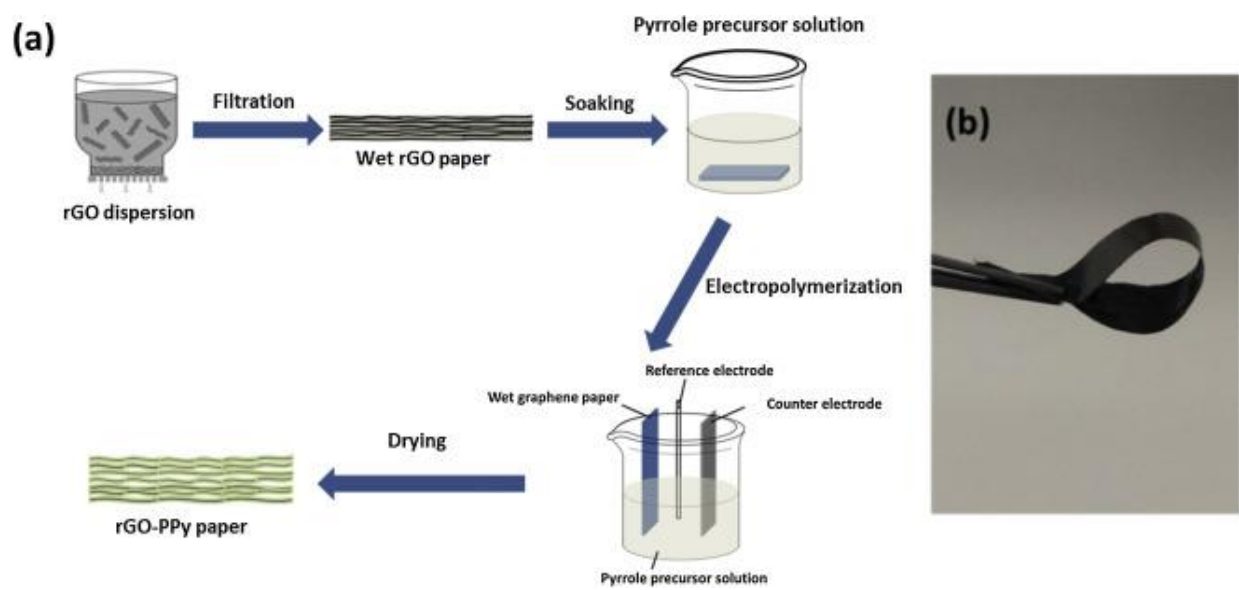
Figure 7 Electrochemical performance of the symmetric supercapacitors using rGO, rGO-PPy 20, rGO-PPy40 or rGO-PPy60 paper electrodes in 1M H<sub>2</sub>SO<sub>4</sub>. (a-d) Charge/discharge curves; (e) Areal capacitance versus current densities; (f) Cycle stability at a current density of 2 A g<sup>-1</sup>.

Figure 8 Ragone plot of rGO-PPy hybrid papers in comparison to the reported graphene-based paper materials.

Figure 9 Nyquist plots (a) (scatter: experimental plots, line: fitting plots), and frequency response (b) of neat rGO or rGO-PPy papers based supercapacitor. (a inset: equivalent circuit model)

Figure 10 (a) Charge discharge curves of rGO-PPy40 based flexible supercapacitor. (b) CVs of rGO-PPy40 based flexible supercapacitor (bending and relaxation state) at a scan rate of 20 mV s<sup>-1</sup>.

**Figure 1**





**Figure 2**

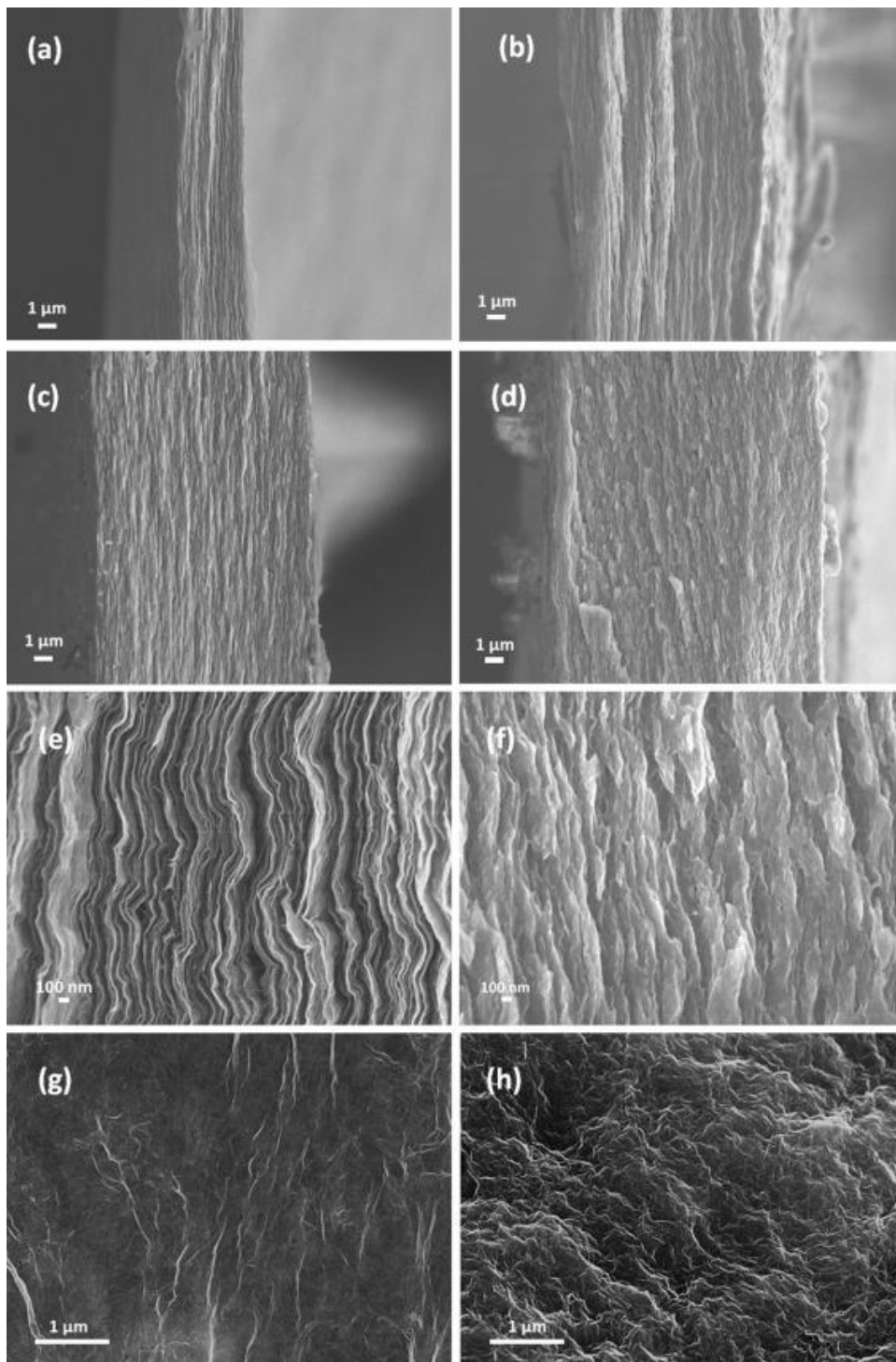


Figure 3

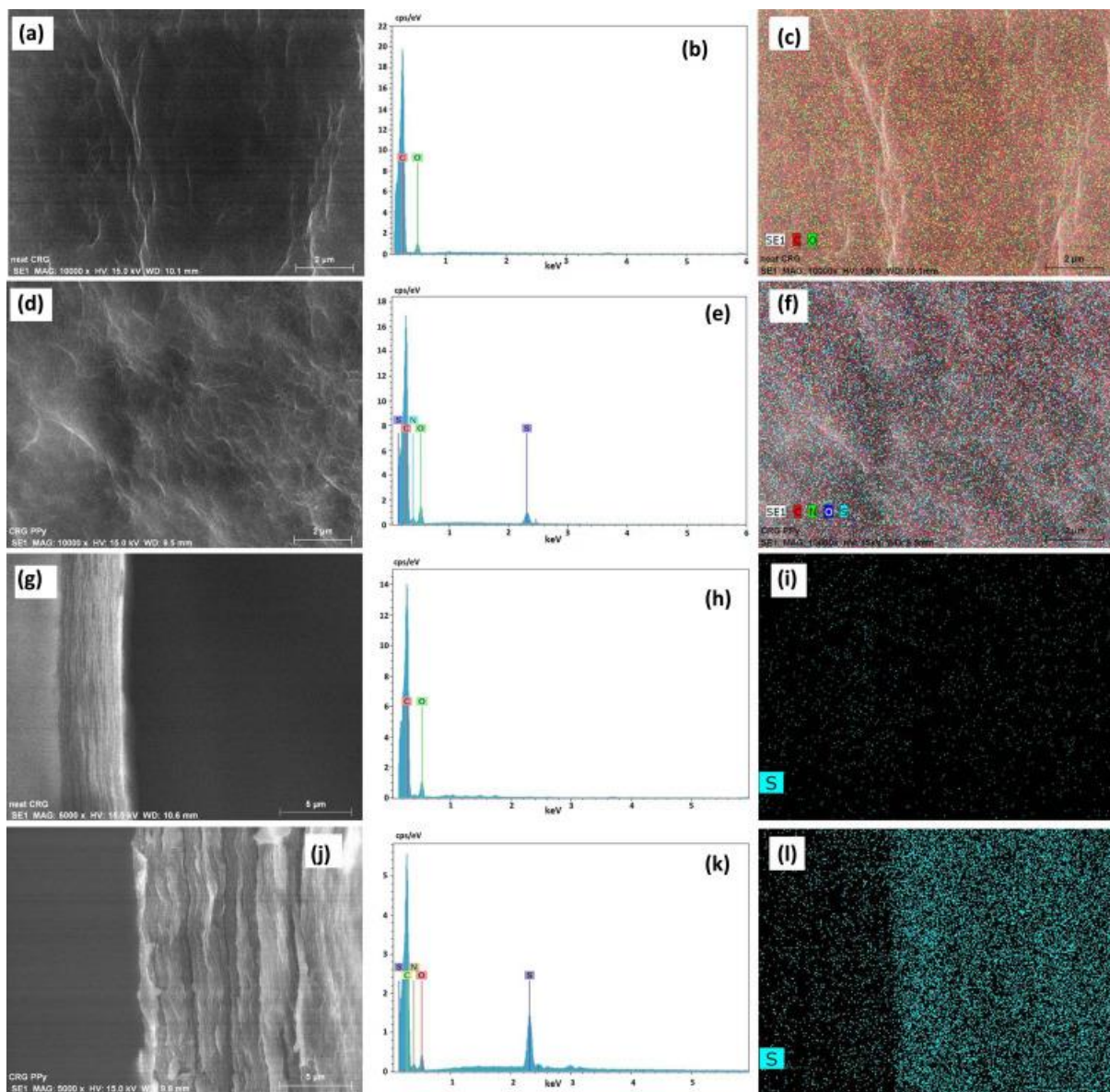


Figure 4

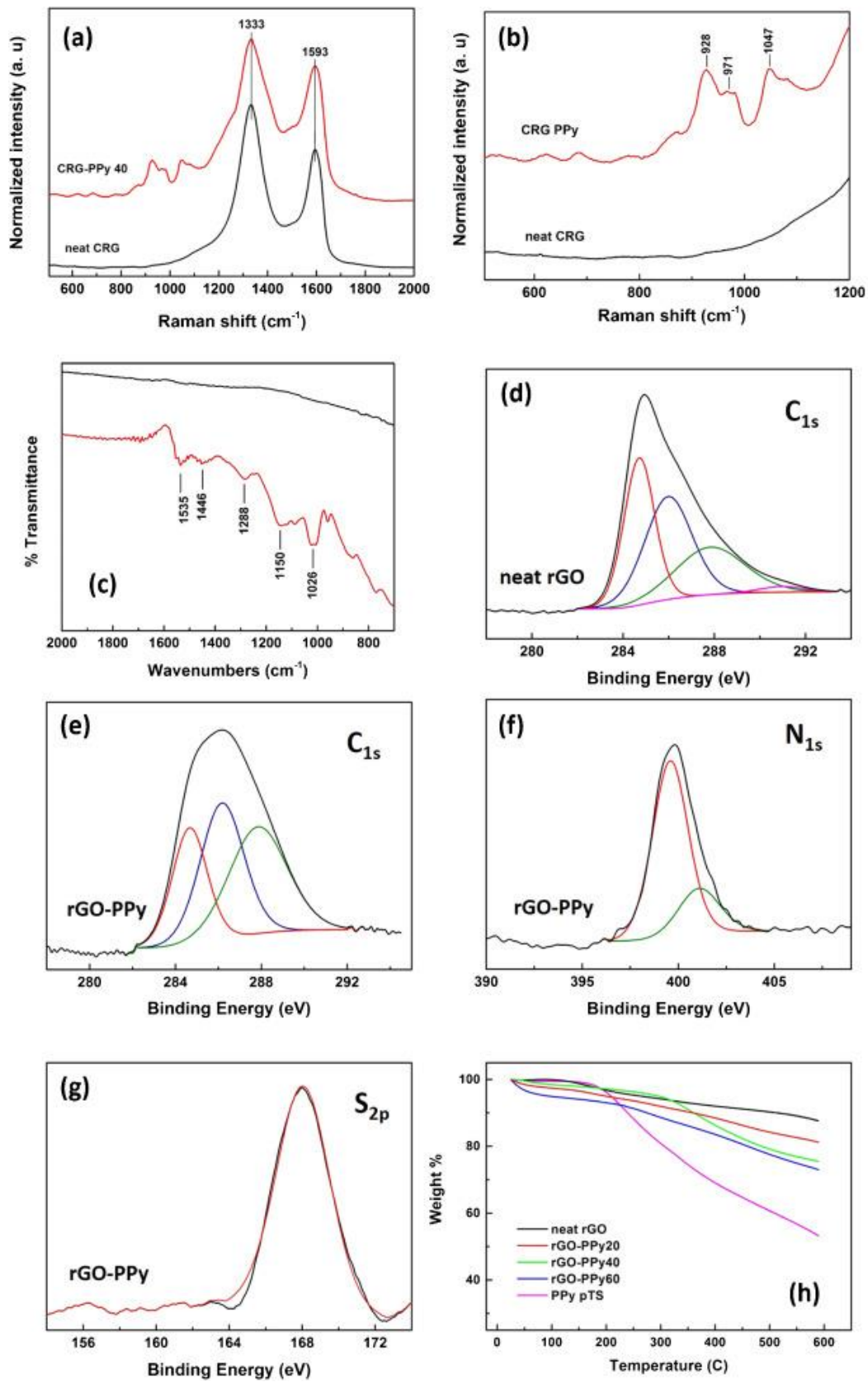


Figure 5

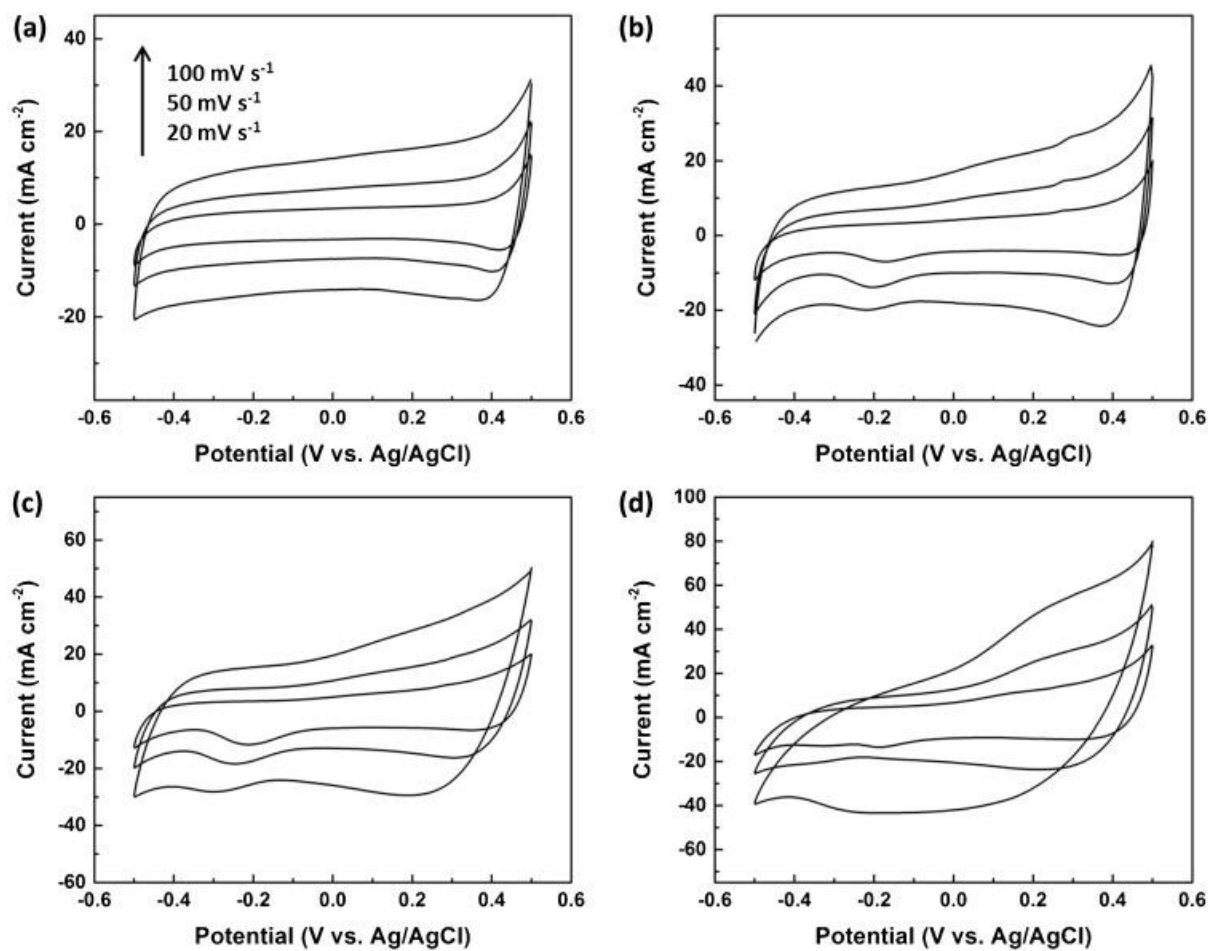


Figure 6

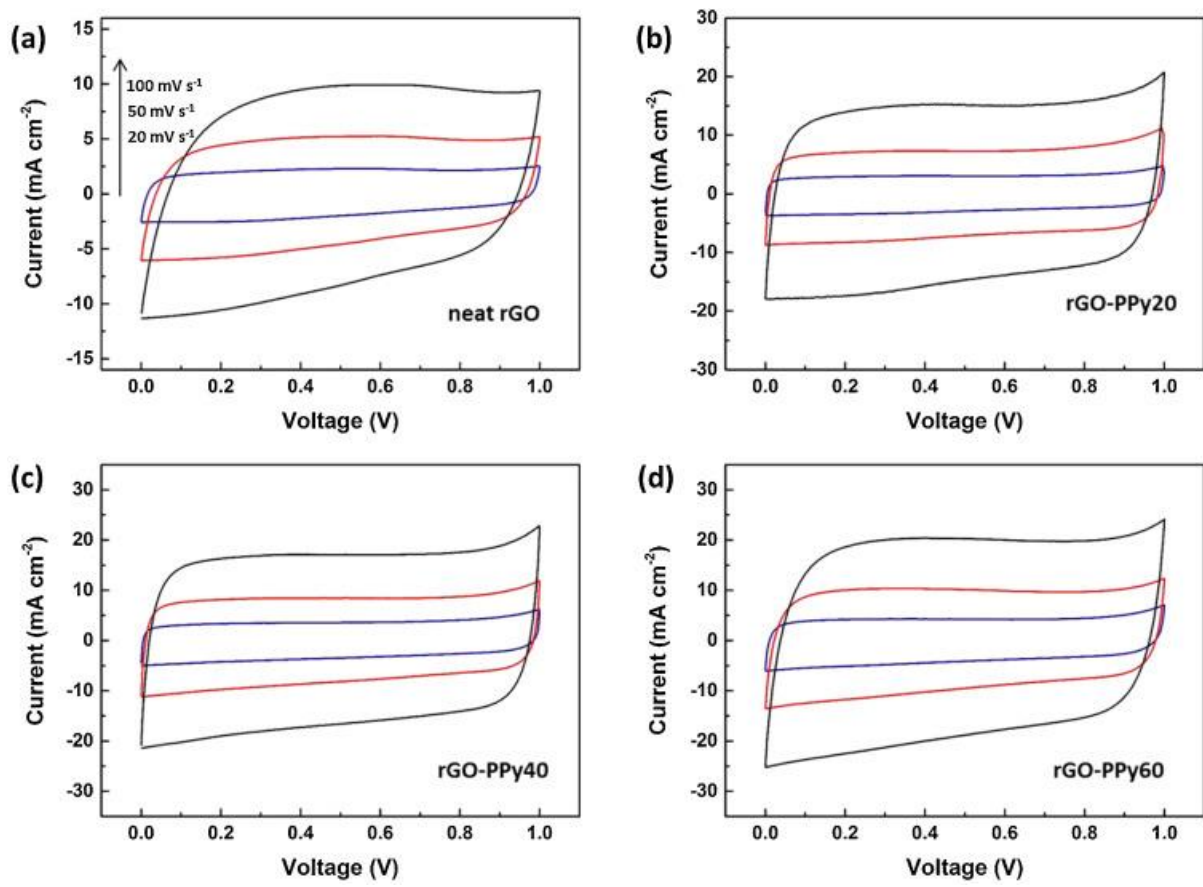




Figure 7

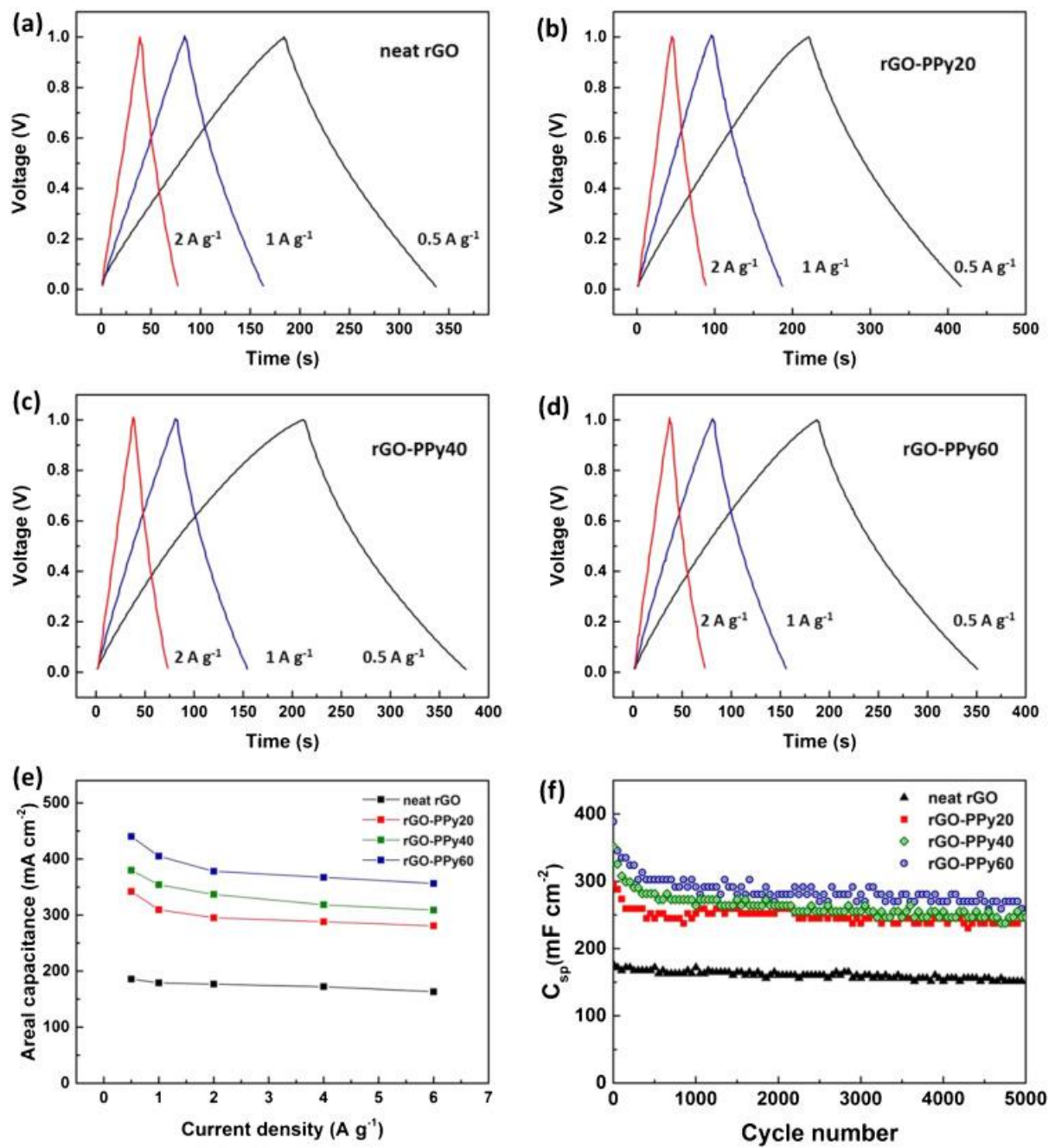


Figure 8

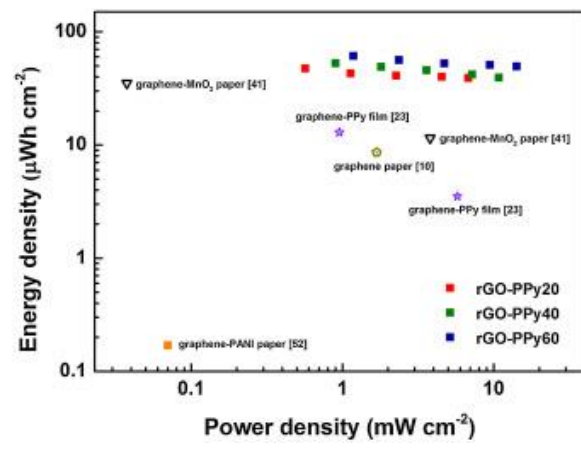


Figure 9

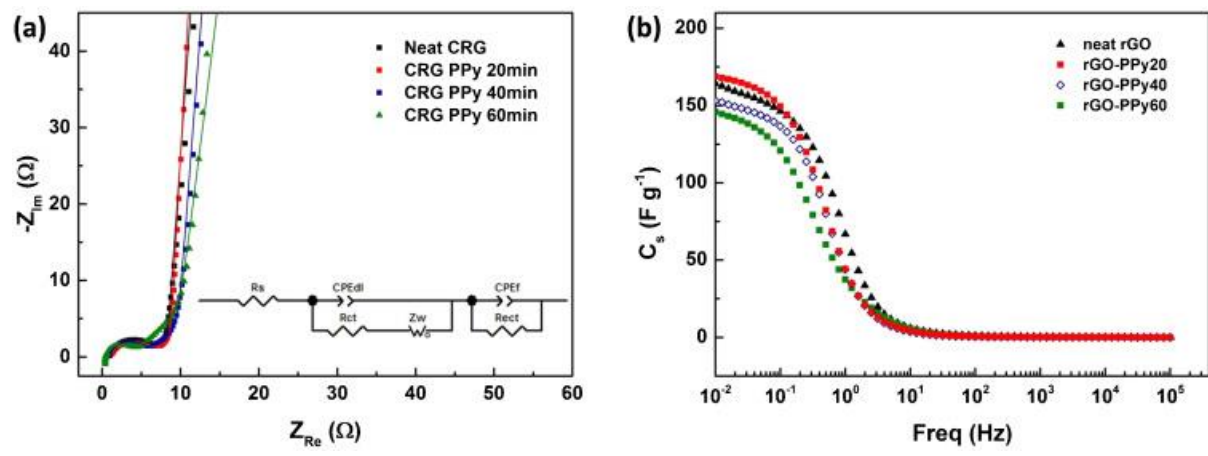




Figure 10

